

Control of two-dimensional excitonic light emission via photonic crystal

This content has been downloaded from IOPscience. Please scroll down to see the full text.

2014 2D Mater. 1 011001

(<http://iopscience.iop.org/2053-1583/1/1/011001>)

View [the table of contents for this issue](#), or go to the [journal homepage](#) for more

Download details:

IP Address: 171.67.216.22

This content was downloaded on 13/04/2014 at 17:16

Please note that [terms and conditions apply](#).

Letter

Control of two-dimensional excitonic light emission via photonic crystal

Sanfeng Wu¹, Sonia Buckley², Aaron M Jones¹, Jason S Ross³,
Nirmal J Ghimire^{4,5}, Jiaqiang Yan^{5,6}, David G Mandrus^{4,5,6}, Wang Yao⁷,
Fariba Hatami⁸, Jelena Vučković², Arka Majumdar⁹ and Xiaodong Xu^{1,3}

¹ Department of Physics, University of Washington, Seattle, WA 98195, USA

² Ginzton Laboratory, Stanford University, Stanford, CA 94305, USA

³ Department of Material Science and Engineering, University of Washington, Seattle, WA 98195, USA

⁴ Department of Physics and Astronomy, University of Tennessee, Knoxville, TN 37996, USA

⁵ Materials Science and Technology Division, Oak Ridge National Laboratory, Oak Ridge, TN 37831, USA

⁶ Department of Materials Science and Engineering, University of Tennessee, Knoxville, TN 37996, USA

⁷ Department of Physics and Center of Theoretical and Computational Physics, University of Hong Kong, Hong Kong, People's Republic of China

⁸ Department of Physics, Humboldt University, D-12489, Berlin, Germany

⁹ Department of Electrical Engineering, University of Washington, Seattle, WA 98195, USA

E-mail: xuxd@uw.edu

Received 14 November 2013, revised 14 January 2014

Accepted for publication 21 January 2014

Published 4 April 2014


2D Materials **1** (2014) 011001

doi:[10.1088/2053-1583/1/1/011001](https://doi.org/10.1088/2053-1583/1/1/011001)

Abstract

Monolayers of transition metal dichalcogenides (TMDCs) have emerged as new optoelectronic materials in the two dimensional (2D) limit, exhibiting rich spin-valley interplays, tunable excitonic effects, and strong light-matter interactions. An essential yet undeveloped ingredient for many photonic applications is the manipulation of its light emission. Here we demonstrate the control of excitonic light emission from monolayer tungsten diselenide (WSe₂) in an integrated photonic structure, achieved by transferring one monolayer onto a photonic crystal (PhC) with a cavity. In addition to the observation of an effectively coupled cavity-mode emission, the suspension effects on PhC not only result in a greatly enhanced (~60 times) photoluminescence but also strongly pattern the emission in the subwavelength spatial scale, contrasting on and off the holes. Such an effect leads to a significant diffraction grating effect, which allows us to redistribute the emitted photons both polarly and azimuthally in the far field

through designing PhC structures, as revealed by momentum-resolved microscopy. A 2D optical antenna is thus constructed. Our work suggests a new way of manipulating photons in hybrid 2D photonics, important for future energy efficient optoelectronics and 2D nano-lasers.

 Online supplementary data available from stacks.iop.org/2DM/1/011001/mmedia

Keywords: transition metal dichalcogenides, 2D semiconductor, photonic crystal, excitonic light emission, optical antenna

Major efforts in optoelectronic research focus on searching for the proper materials and designs for critical components, such as light emitters, optical modulators, converters and detectors. Monolayers of transition metal dichalcogenides (TMDCs), i.e., MX_2 ($\text{M}=\text{Mo}, \text{W}$; $\text{X}=\text{S}, \text{Se}, \text{Te}$), have been regarded as promising candidates for these applications [1], thanks to their outstanding semiconducting behavior in the two-dimensional (2D) limit [2–10] and exceptional ability to convert light into photo-current [11] in an atomically thin structure. Based on these properties, single layer MoS_2 transistors [12], ultrahigh-gain phototransistors [13], ultrasensitive photodetectors [14] and light-emitting diodes (LEDs) [15–18] have already been demonstrated.

Many of the novelties and potential applications of these monolayer TMDCs lie in their excitonic light emissions. A controllable and directional emission in such systems is thus highly desired for developing efficient photonic and optoelectronic components. PhCs, periodic optical nanostructures, and photonic crystal cavities (PhCCs) are powerful platforms for guiding on-chip photons [19], manipulating light emission [20], and enhancing light–matter interactions [21, 22]. A successful integration of 2D TMDCs with PhC structures would provide a powerful way to manipulate their exotic excitonic emissions, as well as represent a novel optoelectronic hybrid capable of harnessing the advantages of both monolayer semiconductors and PhCs.

The idea of utilizing PhCs to modify light emission and enhance quantum yield from a semiconducting emitter has led to fruitful achievements in quantum well LEDs [20, 23, 24]. Figures 1(a) and (b) show typical devices with light emitting materials (multi-quantum wells) embedded into a 2D PhC, which employs its photonic band-gap [23] and diffraction grating effect [24], to redistribute the emitted photons. However, in terms of being compatible with integrated electronic circuits [20], these designs have potential difficulties: (1) it is challenging to fabricate contacts [25] transverse to the light-active material to form electronic elements like transistors; (2) light extraction is limited to the light cone from which light can escape total internal reflection at the air-semiconductor surface; (3) the low-order guide modes in the diffraction grating approach (figure 1(b)) interact poorly with the PhCs, limiting the device performance; (4) a considerable amount ($\sim 30\%$) of the embedded quantum wells are etched away during PhC fabrication (figure 1(a)), also leading to strong non-radiative surface recombination and degradation of the excitonic properties of the quantum well as a result of the fabrication process [20].

In this letter, we present integrated monolayer TMDC/PhC and PhCC photonic devices that overcome the difficulties mentioned above with great control over photon emission. Figure 1(c) shows our design based on a monolayer TMDC, which is placed on top of a 2D

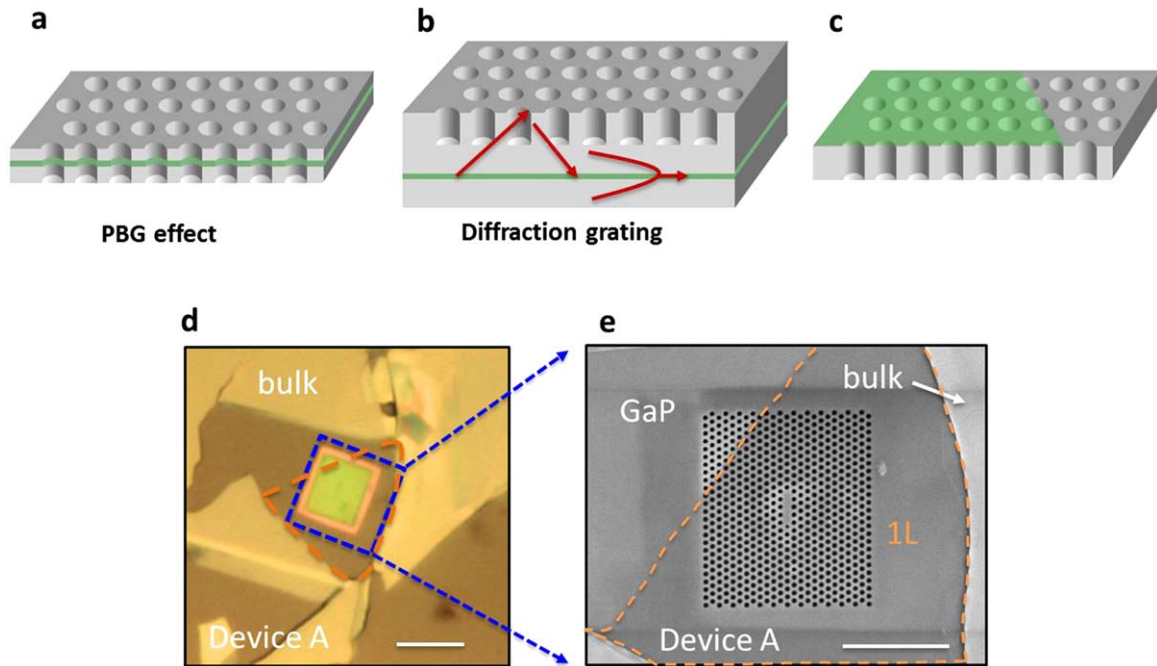


Figure 1. Hybrid monolayer WSe_2/PhC nano-structure. (a), (b) Two types of conventional structures coupling PhC and a light emitting material (green layer), employing photonic band gap effect and diffraction grating effect, respectively. Both structures embed the light active material. The arrows in (b) denote the loss channels from total internal reflection and the low order guided mode. (c) Schematic of coupled TMDC/PhC structure. (d) Optical microscope image of device A. The green area is the PhC and the yellow area is WSe_2 bulk. The monolayer is within the orange dashed line. Scale bar: $5\ \mu\text{m}$. (e) SEM image of the area of interest (indicated by blue dashed line in (d)). Scale bar: $3\ \mu\text{m}$.

photonic crystal (PhC). This geometry provides the following advantages. First, the entire monolayer sheet is open for fabrication of both contacts and gates, allowing for further development of optoelectronic devices. Second, unlike designs which embed the light-active material, there is no loss channel due to total internal reflection and therefore the light cone is the whole upper hemisphere [20]. Third, since the thickness of the semiconducting layer is pushed to the atomic limit, the guided mode is now restricted to the vicinity of the PhC where interactions are strong [20]. Fourth, instead of being destroyed during etching, the monolayer TMDC is placed after PhC fabrication, which preserves the high quality of the emitting layer. These benefits are unprecedented in conventional structures with embedded light emitters.

Monolayer WSe_2 was selected as our light emitting material since it exhibits strong excitonic photoluminescence (PL) (e.g. more than 40 times higher than single layer MoS_2) [26]. To fabricate the hybrid structure, a single layer of WSe_2 was mechanically exfoliated onto a PMMA layer and then transferred to the PhC by standard methods recently developed in 2D material research [27]. Figures 1(d) and (e) show the optical and scanning electron micrograph (SEM) of a typical device (device A). The PhC is fabricated from a 180 nm thick gallium phosphide (GaP) membrane on top of a 800 nm AlGaP sacrificial layer sitting on bulk GaP [28]. A triangular lattice of holes is fabricated in the GaP membrane (see methods section) and a PhCC is defined by omitting holes in the lattice. We choose the lattice parameters so that

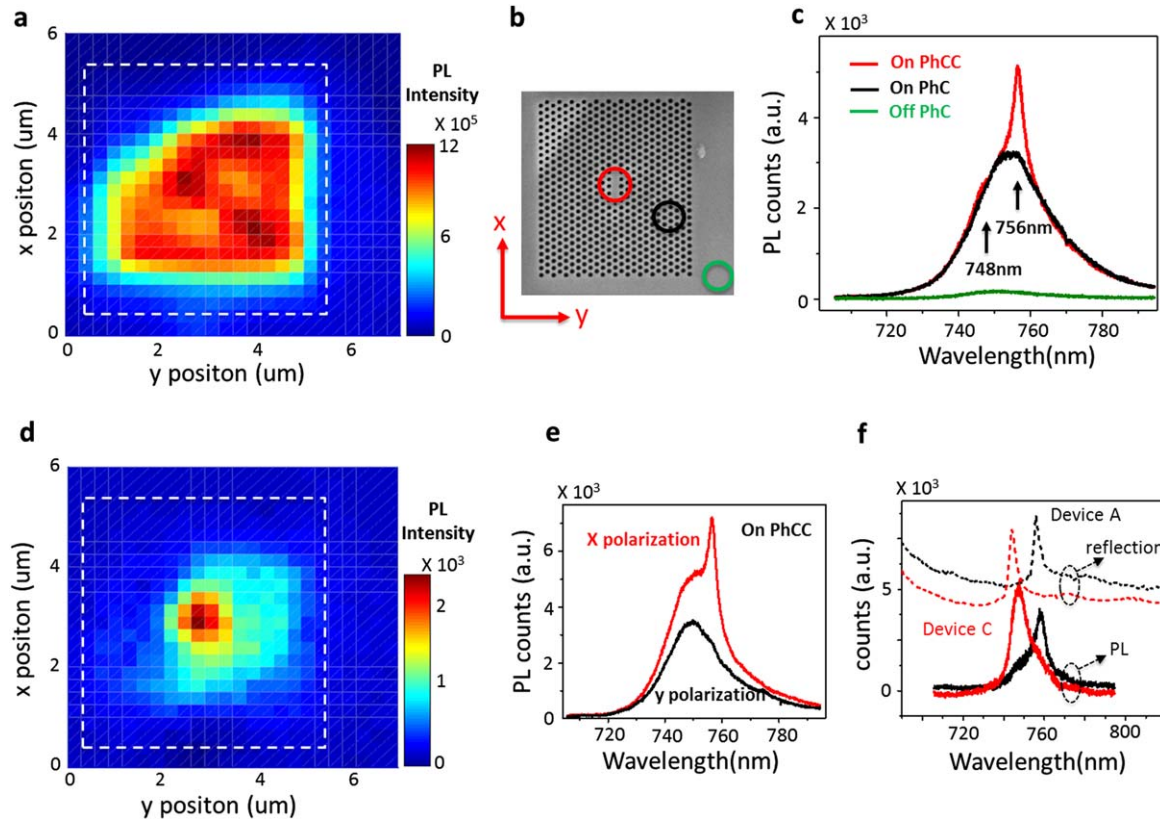


Figure 2. Photoluminescence characterization of the hybrid photonic structures. (a) 2D photoluminescence (PL) intensity color map of device A. (b) The corresponding SEM image of the PhC area with defined axes. (c) Spatially selected PL of device A. The red, black and green spectra are respectively taken from on-PhCC, on-PhC and off-PhC excitation, indicated by the circles in (b). (d) 2D map of peak height difference between PL at 756 nm (on cavity resonance) and 748 nm (off cavity resonance), showing the cavity resonance and mapping out the cavity region. (e) Linear-polarization resolved PL spectra taken for on-cavity excitation, depicting that the corresponding cavity-mode emission is polarized in x direction. (f) Cross-polarized reflection spectra of two devices versus polarized PL spectra, demonstrating the control over the polarized light emission by varying the cavity parameter. Device A and C both have a lattice constant of 200 nm, with device C having a slightly larger hole radius, leading to a blueshift of the cavity resonance.

the PhCC modes match the exciton emission from monolayer WSe_2 . The hole radius, r , is about 50 nm and the lattice constant, a , is 200 nm for devices A and C with a linear four-hole defect, L4. For device B, $r = 100$ nm, $a = 375$ nm with L3. For devices A and C the exciton emission is within the bandgap of the PhC cavity, while for device B the exciton emission is outside the PhC bandgap. After removing the sacrificial layer, the hole depth, D , from the top surface of the PhC to the bottom of the GaP bulk, is estimated to be ~ 980 nm for all devices.

We then study the device via PL measurements pumped by a 660 nm laser focused with a $100\times$ objective (NA=0.95, see methods). Figure 2(a) shows a 2D scanning PL intensity map of device A, where the dashed white line indicates the PhC area. The corresponding sample area is illustrated in figure 2(b). The rectangular shape of the PhC is well-mapped in the PL which

clearly demonstrates that the monolayer on the PhC yields remarkably stronger PL than off the crystal. We selectively plot three spectra taken from off-crystal, on-crystal and on-cavity (circles in figure 2(b)) together in figure 2(c). The total PL intensity on PhC is enhanced 20 times compared to that of off PhC. The highest enhancement ratio obtained among all our devices is about 60 times (see supplementary material, available from stacks.iop.org/2DM/1/011001/mmedia). PL intensity of TMDC monolayers is known to strongly depend on the substrate [2] and the surrounding molecular environment [29]. Our observation indicates that PhCs significantly increase the radiative recombination of excitons in WSe₂, which is mainly due to the suspension effect on the PhC. To clarify such an effect, we have done a control experiment where monolayer WSe₂ is suspended on top of a hole-array only (100 nm in diameter with 1 μm separation between holes). The measurement shows that the PL enhancement from the suspended area is similar to that on-PhC (see supplementary material, figure S5). Therefore, the PL enhancement on PhC can be mainly attributed to the suspension, which strongly patterns the emission in the subwavelength scale. The photonic band-gap effect, which inhibits the spontaneous emission rate laterally and redistributes the light emission into the vertical direction, may also play a role in this device since the light emission falls into the forbidden region [23].

The effective coupling between monolayer and PhC is further revealed by the resonant peak emission at 756 nm (red spectrum in figure 2(c)) when a cavity is present. The presence of this peak indicates coupling to the cavity mode. To clearly show this, we map out the peak amplitude difference between emissions at 756 nm (on cavity mode) and 748 nm (off cavity mode) in figure 2(d). We can see that such peak emission is strongly restricted to the cavity location with ~1 μm lateral size, approximately the length of the cavity. Moreover, PL emission from the cavity is highly polarized in the *x* direction, as shown in figure 2(e). We found that this polarized PL is independent of the polarization of the excitation beam. Such polarization is defined by the corresponding cavity mode. We identify the cavity mode as the *x*-polarized dipole-like mode of the L4 cavity. This mode has a Q factor of ~250 which is sufficient for matching to the broad exciton PL, and strongly radiates in the vertical direction. The Q factor changes to ~180 in excitonic emission after WSe₂ deposition. All the observed modes are identified by a quantitative comparison with the finite-difference time-domain (FDTD) simulations of the cavity [30] (see supplementary material).

By varying the lattice parameters of the PhCC, we are able to tune the emission energy of the polarized PL. To investigate this, device C is designed to have similar Q factor but different lattice parameters (slightly larger hole radius). The PhCCs were characterized by cross-polarized reflectivity measurements [28] (horizontal incident, vertical detection, sample at 45°) before WSe₂ transfer, as shown in the top of figure 2(f). This clearly shows a shift in resonant mode energy with lattice parameters. We get good agreement between this simulation and the cross-polarized reflectivity measurement for the variety of lattice constants fabricated for all the modes. The bottom of figure 2(f) plots the polarized PL (*x*-polarized emission minus *y*-polarized emission) from the WSe₂ on two different PhCCs (devices A and C). The PL emission unambiguously follows the cavity modes. The mechanism for this peak emission can be attributed to the Purcell effect, by which the spontaneous emission rate of the monolayer is increased [31]. In our case, the peak enhancement of the emission rate, i.e., maximum Purcell factor, can be estimated to be $\frac{3}{4\pi^2} \frac{Q}{V} \left(\frac{\lambda_c}{n}\right)^3 \sim 14$, where $\lambda_c \sim 756$ nm is the wavelength of cavity emission, $n \sim 3.1$ is the refractive index of GaP, and $V \sim \left(\frac{\lambda_c}{n}\right)^3$ is the mode volume (the

corresponding optical density of states can be estimated as $\sim \frac{1}{\Delta v V} \sim \frac{n^3}{c\lambda\Delta\lambda} \sim 7.5 \times 10^{-6} \frac{1}{\text{eV nm}^3}$, where $\Delta\lambda$ is the peak width of the cavity emission and $\Delta v = c\Delta\lambda/\lambda^2$. This enhancement, together with the inhibition from the PhC effect, leads to the resonance in the collected PL emission [32].

Based on the effective coupling between monolayer WSe₂ and PhC, we further investigate the far field distribution of light emission from our devices. We find that the emission pattern can be significantly modified by the PhC, through the diffraction grating effect. Momentum resolved microscopy (see methods) is applied to obtain the in-plane (k_x , k_y) momentum distribution of the far field light emission [33]. The in-plane momentum is related to the emission polar angle θ (figure 3) by $\sin(\theta) = k_{\parallel}/k_0$, where $k_{\parallel} = |\mathbf{k}_x + \mathbf{k}_y|$, and $k_0 = 2\pi/\lambda$ is the amplitude of the wave vector of the emitted photon with wavelength λ .

Figure 3(a) plots the normalized PL momentum distribution for samples placed on top of an unpatterned area (off crystal) on the GaP substrate of device A. We also present the data from WSe₂ on SiO₂ substrate in the supplementary material. There is a subtle difference between the two emission patterns. On SiO₂ the light is more vertically directed. Despite these subtleties, both patterns show overall similar behavior with intensity decaying from the center. However, the pattern remarkably changes when the monolayer is on a PhC. Shown in figure 3(b), the exciton emission is highly directed in a ring with polar angle $34^\circ < \theta < 48^\circ$ (defined in figure 3(c)), corresponding to a strong localization of in-plane momentums between $0.55k_0$ and $0.75k_0$. Figure 3(d) compares emission intensities from the different substrates versus polar angle θ along the fixed line $k_x = 0$. For comparison, a Lambertian emission is also presented as the green line. We can see that the light emission from planar substrates tends to have Lambertian-like behavior. However, the PhC drives the emission pattern greatly away from Lambertian to act like an optical antenna [34].

We attribute such antenna-like behavior to the diffraction grating effect of the PhC. Light emission from the periodic pattern interferes in the far field, where the photons coming from different holes experience differing optical path lengths (figure 4(a)). We simulate this effect by considering a 2D triangular diffraction grating. Since the lattice constant a is smaller than λ , the diffraction equation $\sin\theta = m\lambda/a$ only holds for $m = 0$. Considering the etch depth of $D \sim 5\lambda/4$, photons reflected from the bottom surface destructively interfere with those from the top surface, thus suppressing vertical light emission, which corresponds to the primary (1st) maximum of the zeroth order diffraction pattern. Therefore, the secondary (2nd) maximum dominates the diffraction. The 3rd maximum also shows up in experiment, as indicated in figure 3(d). The simulated result is presented in figure 3(e), where experimental parameters are used ($a = 200$ nm, $\lambda = 750$ nm, NA=0.95). The corresponding grating pattern used here is shown in the supplementary material. Our simulation agrees well with the experimental observation, reproducing the antenna pattern and also the emission angle for both 2nd and 3rd diffraction maxima.

In order to demonstrate that the directional emission can be controlled by designing the PhC, we perform a similar measurement on device B where the lattice constant is increased to 375 nm. We found that the emission can not only be directed to certain polar angles, but also in the azimuthal angle, as shown in figure 4(b). Instead of being uniformly distributed along the azimuthal angle, the emission in this device shows interesting islands for both the 2nd (four islands labeled by I) and 3rd (six islands labeled by A) maxima. The change of the grating

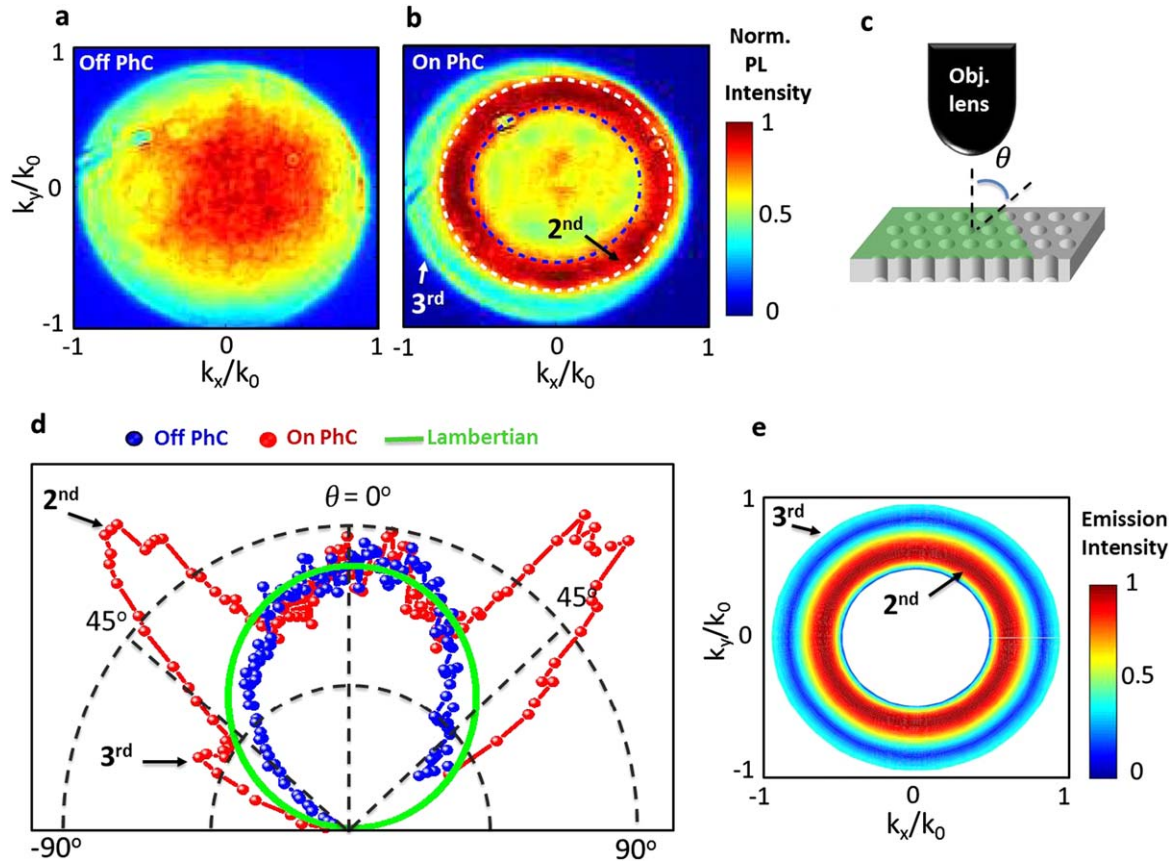


Figure 3. Control of excitonic light emission from monolayer WSe_2 via PhC. (a) Normalized photoluminescence intensity distribution over in-plane momentum space measured by momentum resolved microscopy, when the monolayer is placed on GaP substrate (off crystal area in device A). (b) The same map for sample placed on top of PhC, showing a strikingly different distribution of the light emission. (c) Cartoon plot defining the polar angle of the emission. (d) Polar plot of the emission intensities of the different substrates with $k_x = 0$. As a comparison, the Lambertian type of emission is also plotted. The emission from PhC exhibits an optical-antenna behavior while planar GaP substrate behaves much like Lambertian. (e) Theoretical plot of the momentum distribution of the emission predicted by diffraction grating effect, which agrees very well with the observation.

pattern (see supplementary material, available from stacks.iop.org/2DM/1/011001/mmedia) caused by increasing lattice constant is responsible for the PL pattern. The theoretical simulation, presented in figure 4(c) without any free parameters, is able to capture most of the detailed features observed in the experiment. It is interesting to consider the physical origin of this four-fold emission pattern from a triangular lattice. From the simulation, we find that such emission results from the asymmetric distribution of the responding holes on the edge of the diffraction grating patterns (figure S3(b), two extra holes on two of the six corners). This pattern is a combination of the holes that are emitting collectively and breaks the triangular symmetry.

In summary, our experimental observations show great promise for exploring exotic phenomena and future novel applications based on 2D TMDC/PhC hybrids. Further fabrication of two top gates can lead to an atomically thin LED integrated with a PhCC, which will lead to

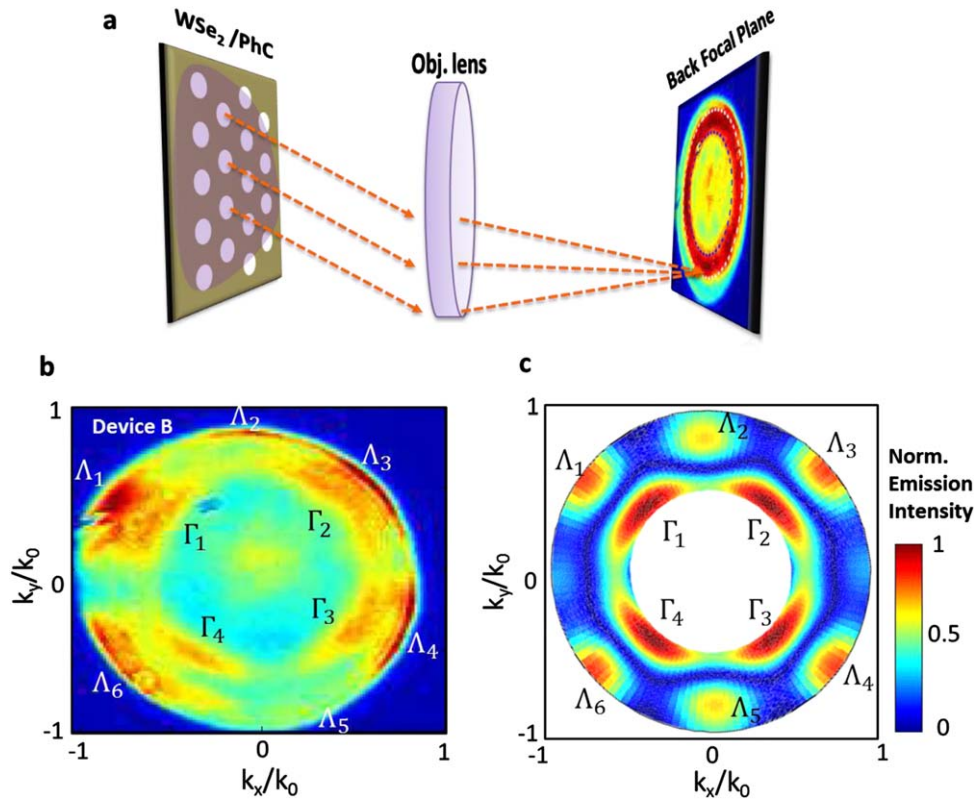


Figure 4. Control of both polar and azimuthal angle of WSe₂ photon emission. (a) Diffraction grating effect and the emission intensity image on the back focal plane of the objective lens. (b) Normalized photoluminescence momentum map for device B with lattice constant $a = 375$ nm, showing that not only the emission over polar angle, but also the azimuthal angle can be redistributed by PhC. (c) Simulation of the emission pattern of device B.

interesting nano-photonic devices such as a single mode LED, potentially with spin or valley polarization, and possible 2D nano-lasers using a high quality factor cavity. The high directionality of the emission also suggests that such hybrid structures may be useful for highly efficient photon sources. The possibility of integration of electronics and photonics in these devices may additionally open up applications in on-chip communications, sensing, and optical computing.

Methods

Device fabrication

A 180 nm GaP membrane was fabricated on top of a 0.8 μm sacrificial layer on a (001)-oriented GaP wafer using gas-source molecular beam epitaxy. A layer of ~ 330 nm electron beam lithography resist (ZEP 520a) was spun on top of the wafer. The pattern was defined using a base dose range of 250–375 $\mu\text{C cm}^{-2}$ using a 100 keV electron beam lithography tool (JEOL JBX 6300). Following development, the pattern was etched deep into the membrane and sacrificial layer using a Cl_2 and BCl_3 chemistry in a plasma etching system. The resist was

removed using microchem remover-PG. The sacrificial layer was then removed using a 7% HF wet etch.

Monolayer WSe₂ was transferred on top of PhC by standard procedures. We first spin-coated polyvinyl alcohol (PVA) (1%) and poly(methyl methacrylate) (PMMA) (950, 6%) on silicon chip followed by baking the chip at 180 °C for 1 min. After we exfoliated the WSe₂ flakes onto the PMMA/PVA/Si stacking substrate. The WSe₂/PMMA membrane was then separated from Si chip by dissolving PVA layer in water. The membrane was scooped up by a loop and the monolayer flake was precisely placed onto the PhC region under microscope, forming a PMMA/monolayer-WSe₂/PhC structure after heating. PMMA layer was removed by a two hour acetone bath.

Momentum resolved microscopy

The momentum resolved microscopy was performed by imaging the back focal plane of the objective lens (Olympus MS Plan 100X/0.95/IC100) which was used for both focusing the laser beam onto sample and collecting the PL signal. The back focal plane image was focused to the open slit of the ANDOR spectrometer by a Bertrand lens with focal length of 150 mm after a telescope setup to optimize the size of the image. The image was then collected by ANDOR newton CCD (1024 × 255 active pixels) by setting the spectrometer grating to zero. The normal PL measurements can be easily coupled to this system. The principle of this momentum resolved measurements can be found in [33].

Acknowledgments

The authors would like to thank Sen Yang for suggestions in momentum resolved measurements and Grant Aivazian for proofreading. This work was mainly supported by DoE, BES, Materials Science and Engineering Division (DE-SC0008145). PhC fabrication was performed in part at the Stanford Nanofabrication Facility of NNIN supported by the National Science Foundation under grant no. ECS-9731293, and at the Stanford Nano Center. SB was supported by a Stanford Graduate Fellowship. SB and JV were also supported by the Presidential Early Award for Scientists and Engineers (PECASE) administered through the Office of Naval Research, under grant number N00014-08-1-0561. NJG, JY and DGM were supported by US DoE, BES, Materials Sciences and Engineering Division.

Author contributions

XX and AM conceived the experiments. SB and AM fabricated and characterized PhCs under JV's supervision. SW prepared and transferred monolayer WSe₂ samples, and performed the measurements with assistance from AMJ. SW analyzed the data and did simulation with discussion from SB, AM, WY, JV and XX. NJG, JY and DGM provided the bulk WSe₂. FH grew the GaP membrane. JSR performed SEM. SW wrote the paper with input from all authors.

References

- [1] Wang Q H, Kalantar-Zadeh K, Kis A, Coleman J N and Strano M S 2012 Electronics and optoelectronics of two-dimensional transition metal dichalcogenides *Nat. Nanotechnol.* **7** 699–712
- [2] Mak K F, Lee C, Hone J, Shan J and Heinz T F 2010 Atomically thin Mo₂: a new direct-gap semiconductor *Phys. Rev. Lett.* **105** 136805
- [3] Splendiani A *et al* 2010 Emerging photoluminescence in monolayer MoS₂ *Nano Lett.* **10** 1271–5
- [4] Xiao D, Liu G-B, Feng W, Xu X and Yao W 2012 Coupled spin and valley physics in monolayers of MoS₂ and other group-VI dichalcogenides *Phys. Rev. Lett.* **108** 196802
- [5] Cao T *et al* 2012 Valley-selective circular dichroism of monolayer molybdenum disulphide *Nat. Commun.* **3** 887
- [6] Mak K F, He K, Shan J and Heinz T F 2012 Control of valley polarization in monolayer MoS₂ by optical helicity *Nat. Nanotechnol.* **7** 494–8
- [7] Zeng H, Dai J, Yao W, Xiao D and Cui X 2012 Valley polarization in MoS₂ monolayers by optical pumping *Nat. Nanotechnol.* **7** 490–3
- [8] Wu S *et al* 2013 Electrical tuning of valley magnetic moment via symmetry control *Nat. Phys.* **9** 149–53
- [9] Gong Z *et al* 2013 Magnetoelectric effects and valley-controlled spin quantum gates in transition metal dichalcogenide bilayers *Nat. Commun.* **4** 15
- [10] Ross J S *et al* 2013 Electrical control of neutral and charged excitons in a monolayer semiconductor *Nat. Commun.* **4** 1474
- [11] Britnell L *et al* 2013 Strong light–matter interactions in heterostructures of atomically thin films *Science* **340** 1311
- [12] Radisavljevic B, Radenovic A, Brivio J, Giacometti V and Kis A 2011 Single-layer MoS₂ transistors *Nat. Nanotechnol.* **6** 147–50
- [13] Zhang W *et al* 2013 Ultrahigh-gain phototransistors based on graphene-MoS₂ heterostructures arXiv:1302.1230
- [14] Lopez-Sanchez O, Lembke D, Kayci M, Radenovic A and Kis A 2013 Ultrasensitive photodetectors based on monolayer MoS₂ *Nat. Nanotechnol.* **8** 497–501
- [15] Sundaram R S *et al* 2013 Electroluminescence in single layer MoS₂ *Nano Lett.* **13** 1416–1321
- [16] Pospischil A, Furchi M M and Mueller F 2013 Solar energy conversion and light emission in an atomic monolayer P-N diode arXiv:1309.7492
- [17] Baugher B W H, Churchill H O H, Yang Y and Jarillo-Herrero P 2013 Optoelectronics with electrically tunable PN diodes in a monolayer dichalcogenide arXiv:1310.1816
- [18] Ye Y, Ye Z, Gharghi M, Zhu H, Zhao M, Yin X and Zhang X 2013 Exciton-related electroluminescence from monolayer MoS₂ arXiv:1305.4235
- [19] Joannopoulos J D, Villeneuve P R and Fan S 1997 Photonic crystals: putting a new twist on light *Nature* **386** 143–9
- [20] David A, Benisty H and Weisbuch C 2012 Photonic crystal light-emitting sources *Rep. Prog. Phys.* **75** 126501
- [21] Majumdar A, Kim J, Vuckovic J and Wang F 2013 Electrical control of silicon photonic crystal cavity by graphene *Nano Lett.* **13** 515–8
- [22] Gan X, Mak K F, Gao Y, You Y, Hatami F, Hone J, Heinz T F and Englund D 2012 Strong enhancement of light–matter interaction in graphene coupled to a photonic crystal nanocavity *Nano Lett.* **12** 5625–31
- [23] Masayuki F *et al* 2005 Simultaneous inhibition and redistribution of spontaneous light emission in photonic crystals *Science* **308** 1296
- [24] Wierer J J Jr, David A and Megens M 2009 III-Nitride photonic-crystal light-emitting diodes with high extraction efficiency *Nat. Photonics* **3** 163–9
- [25] Ellis B, Mayer M, Shambat G, Samiento T, Haller E, Harris J S and Vuckovic J 2011 Ultralow-threshold electrically pumped quantum-dot photonic-crystal nanocavity laser *Nat. Photonics* **5** 297–300

- [26] Zhao W *et al* 2013 Evolution of electronic structure in atomically thin sheets of WS₂ and WSe₂ *ACS Nano* **7** 791–7
- [27] Dean C R *et al* 2010 Boron nitride substrate for high-quality graphene electronics *Nat. Nanotechnol.* **5** 722–6
- [28] Rivoire K, Faraon A and Vuckovic J 2008 Gallium phosphide photonic crystal nanocavities in the visible *Appl. Phys. Lett.* **93** 063103
- [29] Tongay S *et al* 2013 Broad-range modulation of light emission in two-dimensional semiconductor by molecular photoproton gating *Nano Lett.* **13** 2831–6
- [30] Chalcraft *et al* 2007 Mode structure of the L3 photonic crystal cavity *Appl. Phys. Lett.* **90** 241117
- [31] Noda S, Fujita M and Asano T 2007 Spontaneous-emission control by photonic crystal and nanocavities *Nat. Photonics.* **1** 449–58
- [32] Gan X *et al* 2013 Controlling the spontaneous emission rate of monolayer MoS₂ in a photonic crystal nanocavity *Appl. Phys. Lett.* **103** 181119
- [33] Schuller J A *et al* 2013 Orientation of luminescent excitons in layered nanomaterials *Nat. Nanotechnol.* **8** 271–6
- [34] Novotny L and van Hulst N 2011 Antennas for light *Nat. Photonics* **5** 83–90